Railway Dynamics with Curved Contact Patch

Filipe Marques[1](✉), Hugo Magalhães[2,3], João Pombo[2,3], Jorge Ambrósio[3], and Paulo Flores[1]

[1] CMEMS-UMinho, Departamento de Engenharia Mecânica, Universidade do Minho, Campus de Azurém, 4804-533 Guimarães, Portugal
{fmarques,pflores}@dem.uminho.pt
[2] Institute of Railway Research, School of Computing and Engineering, University of Huddersfield, Huddersfield, UK
{h.magalhaes,j.pombo}@hud.ac.uk
[3] IDMEC, Instituto Superior Técnico, Universidade de Lisboa, Av. Rovisco Pais, 1, 1049-001 Lisbon, Portugal
jorge.ambrosio@tecnico.ulisboa.pt

Abstract. The wheel-rail contact modeling is of paramount importance for the dynamics of railway vehicles since it represents the interaction between the vehicle and the track. Although, in most cases, the contact generated occurs between convex surfaces which results in planar contact areas, the contact might take place in concave surfaces when negotiation sharp curves or due to the wear of profiles. In that cases, the resulting contact area is not planar. This work proposes a methodology to determine the shape of the contact patch in a curved surface, where the normal direction varies along its lateral direction. This method is based on a semi-Hertzian approach and discretizes the contact into longitudinal strips. The normal pressure distribution is computed in each strip separately using a non-Hertzian contact model and it is summed in a vector form to obtain the total normal force magnitude. Regarding the tangential forces, a look up table approach is considered. Finally, a trailer vehicle negotiating a curve is used to demonstrate the effectiveness of this methodology.

Keywords: Railway dynamics · Contact forces · Conformal contact · Non-Hertzian

1 Introduction

The utilization of multibody systems methodologies to model the dynamic behavior of railway vehicles has been gaining relevance in their design and development [1]. In that sense, the wheel-rail contact interaction plays a preponderant role since it represents the interface between vehicles and track system. The accurate modeling of the wheel-rail contact is fundamental to analyze the dynamic response of the vehicle, in terms of comfort and safety, for any running conditions, requiring taking into account several complex phenomena that occur during contact [2].

Most of the wheel-rail contact force models available in the literature are limited to their application in planar contact patches, i.e., non-conformal contact cases, or even

M. Pucheta et al. (Eds.): MuSMe 2021, MMS 110, pp. 105–113, 2022.
https://doi.org/10.1007/978-3-030-88751-3_11

to point contact simplification [3, 4]. Although the planar contact assumption covers most of the possible interaction scenarios, in which the rail interacts directly with the tread or flange, when negotiating sharp curves or due to worn profiles, the conformal contact tends to occur in the running profile fillet zone. The common methods of contact search tend to fail in finding a unique solution in a con-formal case, either using elastic or constraint approach.

In this work, a methodology to consider a curved contact between wheel and rail elements is proposed. In the case of interaction between a convex body and a concave body, under the assumption of rigid bodies, an interpenetration region exists, and the effective contact area is smaller due to the elastic deformation of the surfaces. However, in the conformal case, the resultant contact patch tends to have a curved shape [5].

2 Curved Wheel-Rail Contact Model

In the context of the presented methodology, wheels and rails are mathematically represented by parametrized surfaces, i.e., the location of any point on each of surface can be defined by two parameters. The surface of each rail is obtained through the sweep of its cross-section along a given path, which is represented by a set of nodal points and interpolated with a suitable spline. These nodal points define the position and orientation of the rail as function its arc length, s_r. Then, the rail profile is represented by a two-dimensional function, in which the profile vertical coordinate f_r is defined as a function of the surface parameter that defines the lateral rail coordinate, u_r. In turn, since the wheelset is a body of revolution, the wheel surface can be defined by the rotation of its cross-section about its own axis. Thus, any point in the wheel surface is characterized by an angular position and a lateral coordinate. Similar to the rail, the wheel profile is represented by a two-dimensional function, in which the wheel vertical coordinate, f_w, is dependent on the profile lateral position. The schematic representation of this parametrization of the wheel and rail surfaces is given in Fig. 1, in which the superscripts 'L' and 'R' denote the left and right elements, respectively.

The half-space approach is widely employed in the development of most wheel-rail contact theories, for which the only exception is when using the finite element method that is computationally intensive. This concept involves several assumptions, namely (i) the characteristic sizes of the contacting bodies are large compared to the size of the contact patch; (ii) the materials are homogeneous, isotropic and linearly elastic, and (iii) the strains are small, and the inertia effects can be neglected [6]. Having in mind that the size of the contact patch tends to increase due to the conformality between surfaces, the first assumption can be violated. However, the elastic half-space assumption can be kept since it is valid for smaller variations of the contact angle, as it is considered here.

The procedure proposed is here to compute the shape of a curved patch is illustrated in Fig. 2, in which the contact dimension is exaggerated for sake of understandability.

The first step consists of identifying the interpenetration region which limits are obtained with the methodology provided in [3] and denoted by $u_{\mathrm{w,lower}}$ and $u_{\mathrm{w,upper}}$ for the wheel lateral parameter, and by $u_{\mathrm{r,lower}}$ and $u_{\mathrm{r,upper}}$ for the rail lateral parameter. Since the patch is not flat, there is no preferential direction, therefore, the profiles must be parametrized according to their arc length. The wheel potential contact points can

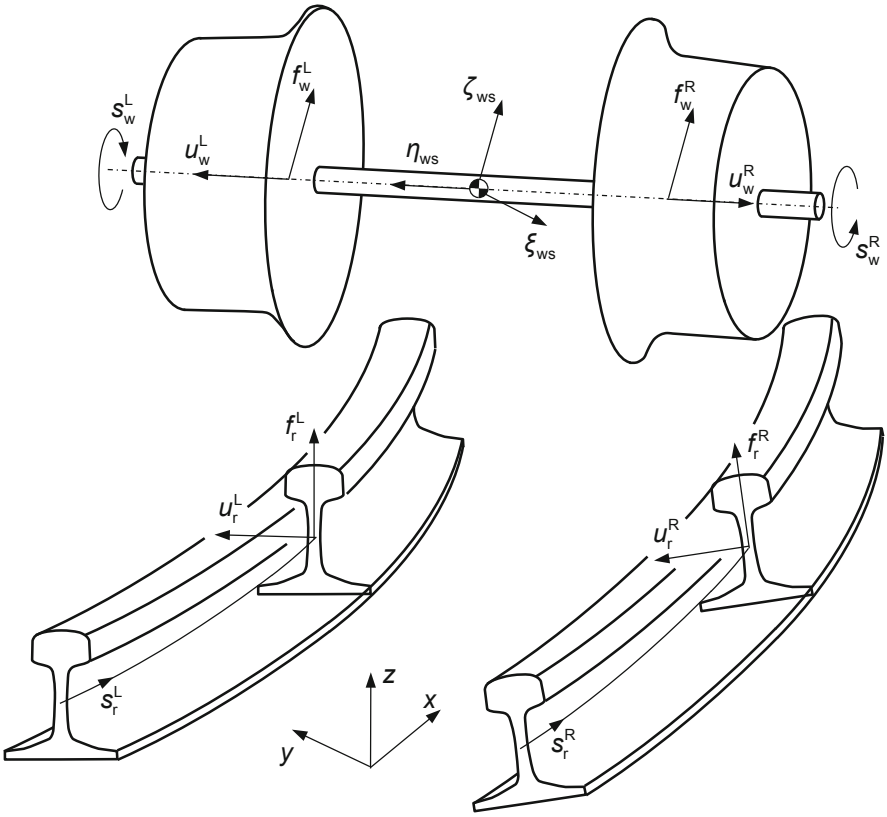

Fig. 1. Schematic representation of the wheel and rail surfaces parametrization

be represented by a three-dimensional curve and the angular parameter, s_w, is given as function of the lateral parameter and yaw angle, α. Hence, to perform this length's parametrization, the wheel has to be projected into the rail profile plane, since the rail is considered an extruded body. This strategy transforms the identification of the contact patch in a two-dimensional problem, which simplifies the process of evaluation the penetration over the patch. Hence, after some mathematical manipulation, the expressions to obtain the arc length for rail and the wheel interpenetration region are

$$L_r(u_r) = \int_{u_{r,\text{lower}}}^{u_r} \sqrt{1 + f_r'}\, \mathrm{d}u_r \tag{1}$$

$$L_w(u_w) = \int_{u_{w,\text{lower}}}^{u_w} \sqrt{\begin{array}{r} -\sin^2\alpha\left(f_w'^4 + 2f_w f_w'^2 f_w'' + 2f_w'^2 + 2f_w f_w''\right) + \cos^2\alpha \\ + f_w'^2 + \tan^2\alpha f_w^2 f_w''^2 \left(\frac{\tan^2\alpha f_w'^2}{1-\tan^2\alpha f_w'^2} + \sin^2\alpha\right) \end{array}}\, \mathrm{d}u_w \tag{2}$$

It must be noticed that the rail's arc length just depends on the profile shape and the boundaries of the interpenetration region, while the wheel's arc length also depends on the yaw angle and, therefore, requires its identification for each wheel-rail configuration. Then, both profiles are discretized in N_S equally sized spaces, as schematized

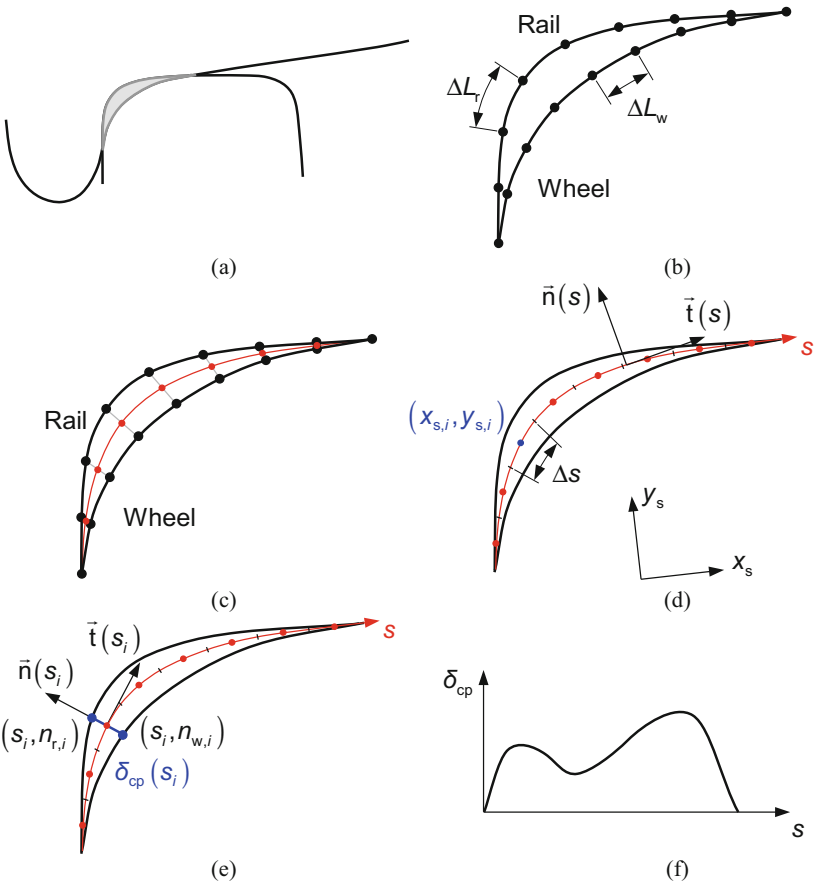

Fig. 2. Definition of the penetration along the interference region in the wheel lateral direction for conformal contacts: (a) interaction of wheel and rail in a conformal region; (b) discretization of the interpenetration zone by its arc length; (c) identification of the contact patch's curved axis; (d) establishment of size and center point of each strip; (e) evaluation of penetration in each strip; (f) representation of the penetration along the interference region

in Fig. 2b. Consequently, the curved surface, s, in which the contact patch is contained can be determined through the evaluation of the middle position between wheel and rail points, as pictured in red in Fig. 2c. Since the points obtained are not necessarily equally spaced in this curve, they have to be resampled and treated in a local coordinate system. Furthermore, $(x_{s,i}, y_{s,i})$ expresses the coordinates of the i^{th} strip, and Δs is the width of each strip, as depicted in Fig. 2d.

A curved axis s is established representing the direction along the contact patch for which the normal and tangential directions are variable. Thus, the normal and tangential vectors are found for each strip as

$$\mathbf{n}_{s,i} = \left\{ -\sin\theta_i \ \cos\theta_i \right\}^{\mathrm{T}} \tag{3}$$

$$\mathbf{t}_{s,i} = \left\{ \cos\theta_i \ \sin\theta_i \right\}^{\mathrm{T}} \tag{4}$$

in which the angle of each strip is defined as

$$\theta_i = \arctan\left(y'_{s,i}\right) \tag{5}$$

where $y'_{s,i}$ denotes the derivative of y_s in $x_{s,i}$ that is calculated from the splines produced. Then, the penetration along the curved contact patch, which is measured in the normal direction of each strip, as represented in Fig. 2e, is evaluated. Both points on rail and wheel which define the limits of the interference of a given strip can be obtained through the intersection between a straight line normal to the patch surface and the rail and wheel profiles, respectively. After determining the intersection points for a given strip, the penetration on that strip, $\delta_{cp}(s_i)$, is the distance between those points. Since the wheel and rail contact is considered locally elastic, their surfaces tend to deform and, therefore, establish an effective contact area which is smaller than the interpenetration region [7]. Hence, the limits of the contact patch, s_s and s_e, are determined by solving the following equation

$$\delta_{cp}(s) = (1-\varepsilon)\delta_{max} \tag{6}$$

where ε is the correction factor, which takes into account the deformation of the contacting surfaces and δ_{max} denotes the maximum penetration in the interference region. This procedure is represented in Fig. 3, and it must be noticed that the first and last strips have a smaller width compared with the remaining ones. For the effective contact zone, the semi-Hertzian approach is considered where the contact pressure distribution is elliptical only for the rolling direction. Thus, the longitudinal size of the i-th strip can be given by the location of the leading edge as

$$x_L(s_i) = \sqrt{2R_w^s(s_i)\left[\delta_{cp}(s_i) - (1-\varepsilon)\delta_{max}\right]} \tag{7}$$

in which R_W^s is the radius of curvature of the wheel surface in the longitudinal direction for a given strip.

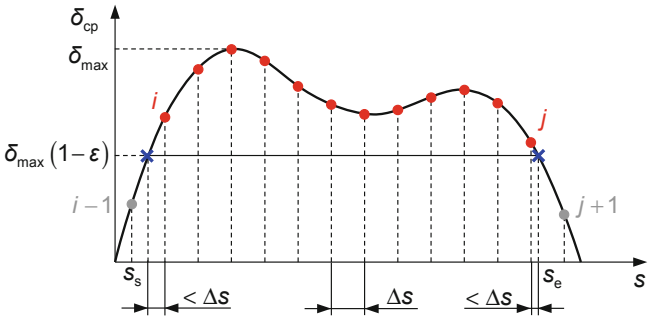

Fig. 3. Schematic representation of the identification of the contact patch limits

Subsequently to the identification of the shape and size of the contact patches, the normal pressure distribution evaluation on each patch is needed. Some of the methods available on the literature depend on the location of the maximum penetration point to calculate the contact pressure [7], which might produce numerical problems when two peaks of penetration are found in the same contact area. A method proposed by Sun et al. [8] is adapted to the curved contact model. In that sense, the contribution of each strip for the normal contact force is computed as

$$f_{\mathrm{n},i} = \frac{\pi^2 E \delta_{\mathrm{cp}}(s_i) x_{\mathrm{L}}^2(s_i) \Delta s}{4\left(1-\sigma^2\right)} \left(\int_{s_{\mathrm{s}}}^{s_{\mathrm{e}}} \int_{-x_{\mathrm{L}}}^{x_{\mathrm{L}}} \sqrt{\frac{x_{\mathrm{L}}^2(\eta) - \xi^2}{\xi^2 + (s_i - \eta)^2}} \, \mathrm{d}\xi \, \mathrm{d}\eta \right)^{-1} \tag{8}$$

where E is the Young's modulus and σ denotes the Poisson ratio. Since the normal direction varies along the contact patch, the normal force magnitude cannot be summed, thus, it is given by the vector sum of the force originated in each strip as

$$\mathbf{f}_{\mathrm{n}} = \sum_{i=1}^{N_{\mathrm{s}}} f_{\mathrm{n},i} \mathbf{n}_{\mathrm{s},i} \tag{9}$$

This model is purely elastic, and a damping component can be added as

$$\mathbf{f}_{\mathrm{n}}^{\mathrm{d}} = \mathbf{f}_{\mathrm{n}} c_{\mathrm{d}} \tag{10}$$

where the damping factor is given as

$$c_{\mathrm{d}} = \begin{cases} c_{\mathrm{e}} & \dot{\delta} \leq -v_0 \\ \left[c_{\mathrm{e}} + (1-c_{\mathrm{e}})\left(3r^2 - 2r^3\right)\right] & -v_0 < \dot{\delta} < v_0 \\ 1 & \dot{\delta} \geq v_0 \end{cases} \quad \text{in which} \quad r = \frac{\dot{\delta} + v_0}{2v_0} \tag{11}$$

where c_{e} expresses the coefficient of restitution, $\dot{\delta}$ represents the penetration velocity and v_0 is a tolerance velocity.

Regarding the evaluation of creep forces and spin moment, a lookup table with a regularization for a simple double-elliptical contact region, based on CONTACT software, is considered [9]. This lookup table requires, as input variables, the parametrized spin creepage, semi-axes ratio, creepage angle, parametrized creepage modulus and shape number. An enhanced version of this lookup table is used, in which its discretization was obtained after minimizing the interpolation error [10].

3 Example of Application

A multibody model of trailer vehicle negotiating a left curve is utilized as example of application of the proposed methodology for the wheel-rail contact model. This model includes 11 rigid bodies, namely 4 wheelsets, 4 axleboxes, 2 bogie frames and the carbody. All details of this model can be found in [11]. The vehicle starts the simulation with a forward velocity of 18.3 m/s and a lateral misalignment of 2 mm with respect to the track centerline to promote some hunting motion.

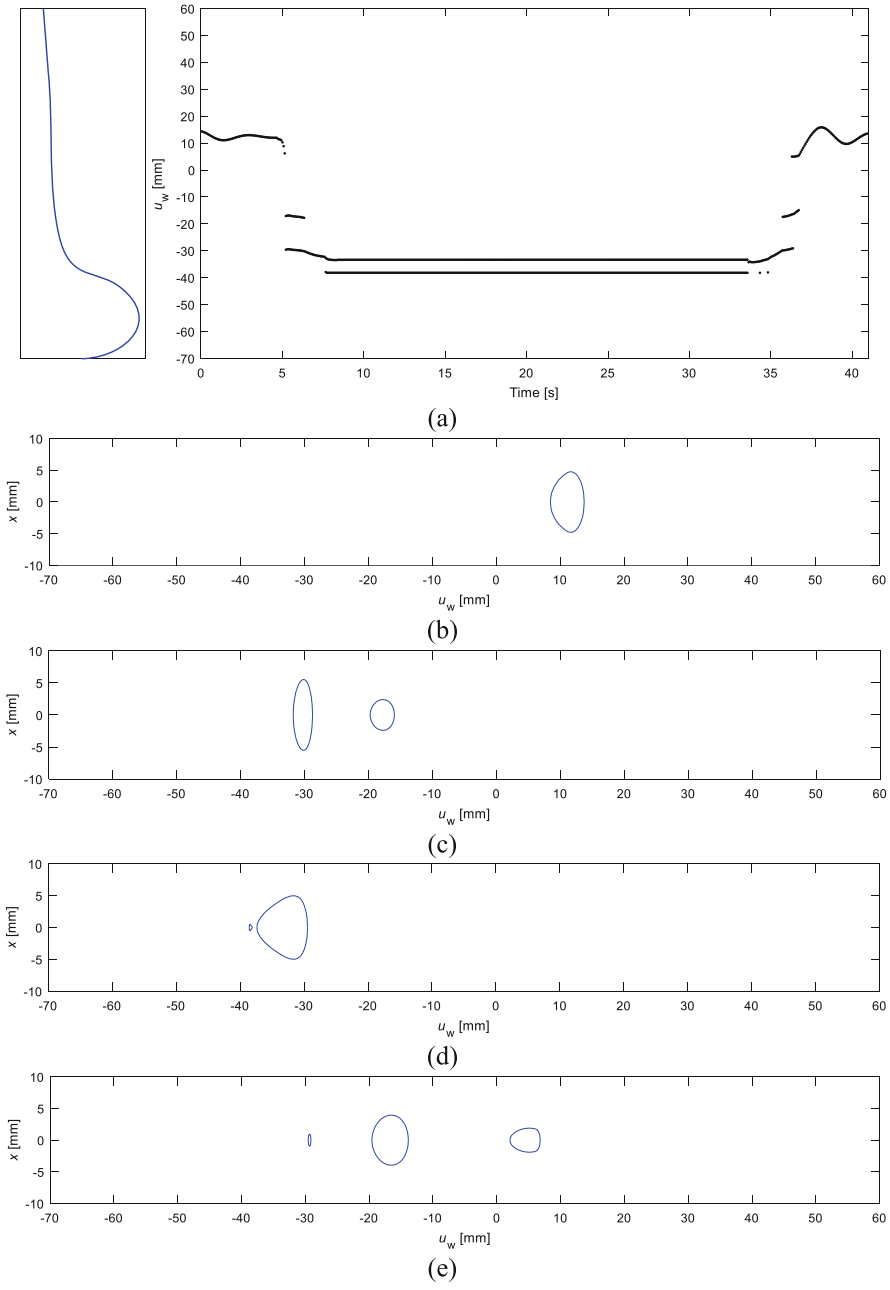

Fig. 4. Representation of (a) the location of the main contact point for each patch and their shape for (b) $t = 1$ s (c) $t = 6$ s (d) $t = 20$ s and (e) $t = 36.4$ s for the right wheel of the leading wheelset.

To analyze the obtained results, the contact in the right wheel of the leading wheelset is examined in detail, since it is external to the curve and, therefore the contact can occur in the wheel transition zone. Figure 4a shows the location of the contact points on the wheel profile during the simulation. From the results, it is concluded that the rail interacts with the wheel transition zone during negotiation where two different contact patches are identified. The different shapes of contact patches determined are displayed in Figs. 4b–e, where four different instants of simulation are considered. Figure 4d exhibits the most non-elliptical contact scenario and coincides with the location in which the wheel presents a concave surface.

4 Conclusions

A method for the determination of a curved contact patch on the interaction between wheel and rail surfaces is presented in this work. This methodology considers that normal contact direction might vary along lateral direction of the contact area and determines the local penetration based on that assumption. A non-Hertzian method for the normal pressure evaluation is adapted to be applied in the curved contact. This contact model has been applied to a dynamic simulation and demonstrated to be effective in the determination of the contact patches and corresponding forces.

Acknowledgments. The first author is supported by the Portuguese Foundation for Science and Technology (FCT) under grant PD/BD/114154/2016, MIT Portugal Program. This work has been supported by FCT with the reference project POCI-01-0145-FEDER-028424, by FEDER funds through the COMPETE 2020 - Programa Operacional Competitividade e Internacionalização. This work has been also supported by Portuguese Foundation for Science and Technology, under the national support to R&D units grant, with the reference project UIDB/04436/2020 and UIDP/04436/2020, as well as through IDMEC, under LAETA, project UIDB/50022/2020.

References

1. Bruni, S., Meijaard, J.P., Rill, G., Schwab, A.L.: State-of-the-art and challenges of railway and road vehicle dynamics with multibody dynamics approaches. Multibody Syst. Dyn. **49**(1), 1–32 (2020). https://doi.org/10.1007/s11044-020-09735-z
2. Meymand, S.Z., Keylin, A., Ahmadian, M.: A survey of wheel-rail contact models for rail vehicles. Veh. Syst. Dyn. **54**(3), 386–428 (2016)
3. Marques, F., Magalhães, H., Pombo, J., Ambrósio, J., Flores, P.: A three-dimensional approach for contact detection between realistic wheel and rail surfaces for improved railway dynamic analysis. Mech. Mach. Theory **149**, 103825 (2020)
4. Magalhães, H., et al.: Implementation of a non-Hertzian contact model for railway dynamic application. Multibody Syst. Dyn. **48**(1), 41–78 (2019). https://doi.org/10.1007/s11044-019-09688-y
5. Vollebregt, E.: Detailed wheel/rail geometry processing with the conformal contact approach. Multibody Syst. Dyn. **52**(2), 135–167 (2020). https://doi.org/10.1007/s11044-020-09762-w
6. Vollebregt, E., Segal, G.: Solving conformal wheel-rail rolling contact problems. Veh. Syst. Dyn. **52**(S1), 455–468 (2014)

7. Piotrowski, J., Kik, W.: A simplified model of wheel/rail contact mechanics for non-Hertzian problems and its application in rail vehicle dynamic simulations. Veh. Syst. Dyn. **46**(1–2), 27–48 (2008)
8. Sun, Y., Zhai, W., Guo, Y.: A robust non-Hertzian contact method for wheel–rail normal contact analysis. Veh. Syst. Dyn. **56**(12), 1899–1921 (2018)
9. Piotrowski, J., Liu, B., Bruni, S.: The Kalker book of tables for non-Hertzian contact of wheel and rail. Veh. Syst. Dyn. **55**(6), 875–901 (2017)
10. Marques, F., et al.: On the generation of enhanced lookup tables for wheel-rail contact models. Wear, **434–435**, 202993 (2019)
11. Marques, F.: Modeling complex contact mechanics in railway vehicles for dynamic reliability analysis and design. Ph.D. thesis, Universidade do Minho (2020)